Annals of Nuclear Energy 36 (2009) 1440–1449

Contents lists available at ScienceDirect

Annals of Nuclear Energy

journal homepage: www.elsevier.com/locate/anucene

An improved three-dimensional wavelet-based method for solving the first-order Boltzmann transport equation

Youqi Zheng, Hongchun Wu, Liangzhi Cao *

School of Nuclear Science and Technology, Xi'an Jiaotong University, Xi'an, Shaanxi 710049, China

ARTICLE INFO

Article history:
Received 24 December 2008
Received in revised form 30 April 2009
Accepted 5 June 2009
Available online 28 June 2009

ABSTRACT

A new angular discretization scheme based on the Daubechies' wavelets has been developed in recent studies. A decoupled S_N and wavelet expansion method was proposed. This paper discusses the limitations and improvements of this decoupled scheme. The scaling function, instead of the wavelet function, is applied as the basis function. It significantly improved the efficiency and computational stability. A new series of wavelets on the interval are applied instead of the 'wrapped wavelets', which eliminate the edge effect in the angular subdomain scheme. Based on the improvements, a wavelet-based neutron transport code package WAVTRAN is developed and the previous work is extended to the three-dimensional calculation and anisotropic scattering calculation. Numerical results demonstrate that the improvements are effective. Further investigations demonstrate that the wavelet-based angular discretization scheme is more powerful than the traditional ones in some highly anisotropic angular flux problems.

1. Introduction

The wavelet functions have recently been applied in the angular discretization of Boltzmann transport equation. To our knowledge, a spline wavelet representation of the polar angular variable in one-dimensional transport problems by Carron (1999) was the first attempt in this field. Buchan (2005) applied the spherical wavelets to discretize both of the polar and azimuthal variables. The angular flux was represented over an octahedron and the multi-resolution analysis (MRA) was taken based on the octahedron to construct the wavelet bases. The Daubechies' wavelets were applied in the angular discretization by Cho and Cao (2006) based on the SAAF (Self-Adjoint Angular Flux) equation. Compared with other wavelets, the Daubechies' wavelets possess strong capability in representing the peaky and discontinuous function, which has been found in recent investigations of the angular flux distribution.

Previous study (Cao et al., 2008) considered a decoupled S_N (discrete ordinate method) and wavelet expansion method in the angular discretization of first-order Boltzmann transport equation. However, several limitations made the new method difficult in further applications. Firstly, the wavelet function was applied as the basis function in the initial form. Therefore, the wavelet expansion coefficients were coupled intensively, even though only the azimuthal variable is expanded by the bases. It might induce the instability in the decoupling of wavelet expansion coefficients. The second problem is the implementation of forcing the basis function on the interval, in which the 'wrapped wavelets' (Newland, 1993) were applied. The wavelets on the interval by use of this transformation induce the edge effect inevitably. It causes the discontinuation of angular flux in the adjacent regions of angular subdomains and affects the accuracy of outcomes.

We start our work for developing the method by removing the edge effect and enhancing the stabilization of decoupling. Based on the previous work on the decoupled S_N and wavelet expansion method, the scaling function, instead of the wavelet function, is applied to expand the azimuthal variable. The scaling function is an approximation which operates in a projection space. With the property of compact support, the wavelet expansion coefficients in the projection space are coupled sparsely, which favors the numerical calculations. Secondly, the wavelets on the interval are applied to replace the 'wrapped wavelets'. This is a significant development of the orthonormal wavelet bases, which is especially suitable for the expansion in a subdomain scheme. Therefore, the edge effect induced by the 'wrapped' wavelet expansion is eliminated and an exact angular flux reconstruction becomes feasible.

A three-dimensional model is constructed to investigate the applicability of decoupled S_N and wavelet expansion method in multi-dimensional calculations. Furthermore, the anisotropic scattering in multi-dimensional calculations is considered to make the method more consummate. The wavelet expressions of macro scattering cross-section in the angular subdomains are deduced based on the Legendre polynomial expansion. Arbitrary order of anisotropic scattering is permitted theoretically. A multi-group

* Corresponding author. Tel.: +86 29 8266 3285; fax: +86 29 8266 7802.
E-mail address: caoliangzhi@gmail.com (L. Cao).

0306-4549/$ - see front matter © 2009 Elsevier Ltd. All rights reserved.
doi:10.1016/j.anucene.2009.06.006

neutron transport calculation code package WAVTRAN is developed based on the method. Various neutron transport problems are analysed to demonstrate the validity and advantage of the improved model.

The paper is outlined as follows, in Section 2, as a background, a fundamental introduction of the scaling function and its construction on the interval is described. The model of the decoupled S_N and wavelet expansion method is deducted in Section 3. The applications of this model in neutron transport solutions are given in Section 4. Finally, in Section 5, the conclusions are drawn close the paper.

2. The fundamental of wavelets

2.1. The introduction of wavelets and scaling function

The wavelet function $\psi(t)$ is denoted as a type of function which satisfies

$$\int_{-\infty}^{\infty}\psi(t)dt=0 \quad \text{and} \quad \psi(t)\in L^2(R) \tag{1}$$

The advantage of wavelets is that, compared with other functions like sine and cosine, the individual wavelet function is localized in both space and frequency. This particular kind of dual localization renders large classes of functions spare to high accuracy, when transformed into the wavelet domain. From this property, wavelets are becoming a useful tool in various fields.

The constructions of recent wavelets start with the MRA as well as several algorithms in vision decomposing and reconstruction. As in the wavelet theory, the wavelet functions $\psi_{n,k}(t)$ are generated by a dilation and translation operation such as

$$\psi_{n,k}(t)=2^{n/2}\psi(2^n t-k) \tag{2}$$

for the integer n and k, which denote the dilation and translation, respectively. Simultaneously, the scaling functions $\varphi_{n,k}(t)$, which are applied to generate the wavelet functions, have the same form for $\varphi_{n,k}\in L^2(R)$ as

$$\varphi_{n,k}(t)=2^{n/2}\varphi(2^n t-k) \tag{3}$$

The relationship of wavelet function and scaling function is called two-scale relation as

$$\varphi(t)=\sum_k c_k\varphi(2t-k) \tag{4}$$

and

$$\psi(t)=\sum_k d_k\varphi(2t-k) \tag{5}$$

If the two-scale relation is restricted by finite sums, the scaling function and wavelet function have compact supports. In additional, if ψ is required to generate orthonormal bases, the relationship of expansion coefficients is

$$d_k=(-1)^k c_{1-k} \tag{6}$$

In this paper, the orthonormal compactly supported wavelets constructed by Daubechies (1992) are applied, including the scaling function and wavelet function. The scaling function $\varphi_{n,k}(t)$ and wavelet functions $\psi_{n,k}(t)$ have the following relationships and compact supports:

$$\begin{aligned}&\varphi_{n,k}(t)=\sum_{j=2k}^{2N+2k-1}c_{j-2k}\varphi_{n+1,j}(t) \quad \text{support}\\ &(\varphi_{n,k}(t))=[2^{-n}k,2^{-n}(k+2N-1)]\end{aligned} \tag{7}$$

and

$$\begin{aligned}&\psi_{n,k}(t)=\sum_{j=2k-2N+2}^{2k-1}(-1)^j c_{1-j+2k}\varphi_{n+!,j}(t) \quad \text{support}\\ &(\psi_{n,k}(t))=[2^{-n}(k+1-N),2^{-n}(k+N)]\end{aligned} \tag{8}$$

where n is called the dilation order and N is called the Daubechies order.

2.2. The Daubechies' wavelets on the interval

The goal of wavelet transform is to decompose arbitrary function $f(t)$ into an infinite summation of wavelets at different scales according to the expansion

$$f(t)=\sum_{n=-\infty}^{\infty}\sum_{k=-\infty}^{\infty}a_{n,k}\psi_{n,k}(t) \tag{9}$$

Usually, the function $f(t)$ is defined on a given interval. It forces the basis function to be defined on the same interval. The most common operation is to normalize the variable on a unit interval, i.e., $0\leqslant x<1$. Therefore, not only the scaling functions but also the wavelet functions are usually restricted to accord the unit interval.

Several methods are developed to restrict the Daubechies' wavelets on the interval. The 'wrapped' Daubechies' wavelets are the most widely used in the numerical methods. Guven and Bayazitoglu (2003) applied this method in solving the radiative transfer equation and demonstrated its feasibility in the angular discretization. The 'wrapped' technique is a process of circular wavelet transform, which divides the wavelets which overlap the boundaries into two parts. The wavelets in the interval are reserved with the others forced to be zero. Considering different contributions from different wavelets, a new set of wavelets is obtained in the process of 'wrapped around'. However, further investigation presents a puzzle encountered in the angular subdomain scheme, which is induced by the edge effect. Even though it affects little in general problems, it is a disadvantage in the further usage of wavelets.

Another approach is to construct a new set of essential wavelets on the interval. Cohen and Daubechies (1993) constructed the set of Daubechies' wavelets by use of fast wavelet transforms. The technique starts with the constructions of wavelets on the boundaries, which are defined as in Eqs. (10), (11) and Eqs. (12), (13) on the left boundary and right boundary, respectively.

$$\varphi_{n,k}^{left}=\sum_{l=0}^{N-1}H_{k,l}^{left}\varphi_{n+1,l}^{left}+\sum_{m=N}^{N+2k}h_{k,m}^{left}\varphi_{n+1,m} \tag{10}$$

$$\psi_{n,k}^{left}=\sum_{l=0}^{N-1}G_{k,l}^{left}\varphi_{n+1,l}^{left}+\sum_{m=N}^{N+2k}g_{k,m}^{left}\varphi_{n+1,m} \tag{11}$$

$$\varphi_{n,k}^{right}=\sum_{l=-N}^{-1}H_{k,l}^{right}\varphi_{n+1,l}^{right}+\sum_{m=-N-1}^{-N-1+2k+2}h_{k,m}^{rihgt}\varphi_{n+1,m} \tag{12}$$

$$\psi_{n,k}^{right}=\sum_{l=-N}^{-1}G_{k,l}^{right}\varphi_{n+1,l}^{right}+\sum_{m=-N-1}^{-N-1+2k+2}g_{k,m}^{rihgt}\varphi_{n+1,m} \tag{13}$$

where φ and ψ stand for the scaling function and wavelet function, respectively. H, h, G and g denote the filter coefficients, which are defined by Cohen and Daubechies in the literature (1993).

The Daubechies' wavelets on the interval are constructed in two steps. Firstly, the wavelets which overlap the boundaries are removed form the initial set of wavelets. Then, $N-1$ new wavelets are added to the remained set on each boundary. Here N denotes the Daubechies order. The new set of Daubechies' wavelets reserves main properties of initial Daubechies' wavelets such as orthonormality and compact support. Moreover, it avoids the potential effect close to the edge regions, which is important in the high-precision reconstruction.

2.3. The scaling function expansion

Suppose we define

$$V_n = closure < \varphi_{n,k} : k \in Z > \tag{14}$$

and

$$W_n = closure < \psi_{n,k} : k \in Z > \tag{15}$$

The scaling function and wavelet function have the following subspace relations:

$$\varphi_{n,k} \in V_n, \psi_{n,k} \in W_n \tag{16}$$

$$\ldots V_{-1} \subset V_0 \subset V_1 \subset V_2 \ldots, V_n = V_{n-1} \oplus W_{n-1} \tag{17}$$

and

$$\overline{\bigcup_n V_n} = L^2(R), \quad \bigoplus_n W_n = L^2(R) \tag{18}$$

Based on the wavelets, an expansion of the $L^2(R)$ function $f(t)$ can be given as

$$f(t) = \sum_{k=-\infty}^{\infty} a_k \phi(t-k) + \sum_{n=0}^{\infty} \sum_{k=-\infty}^{\infty} a_{n,k} \psi(2^n t - k) \tag{19}$$

where ψ is the wavelet function and φ is the scaling function. By use of the 'wrapped' wavelet functions, Eq. (19) can be written in the following equivalent form on the interval:

$$f(t) = a_0 + \sum_n \sum_k a_{2^n+k} \psi(2^n t - k) \quad 0 \leqslant x < 1 \tag{20}$$

From Eq. (20), we know that the wavelet expansion derives from a sum of wavelet functions in different levels or (more precisely) scales. Namely, the function is spanned by a series of subspaces as described in Eq. (18). Suppose a projection of $f(t)$ in the subspace V_n can be denoted as

$$f_n = P_n f \in V_n \tag{21}$$

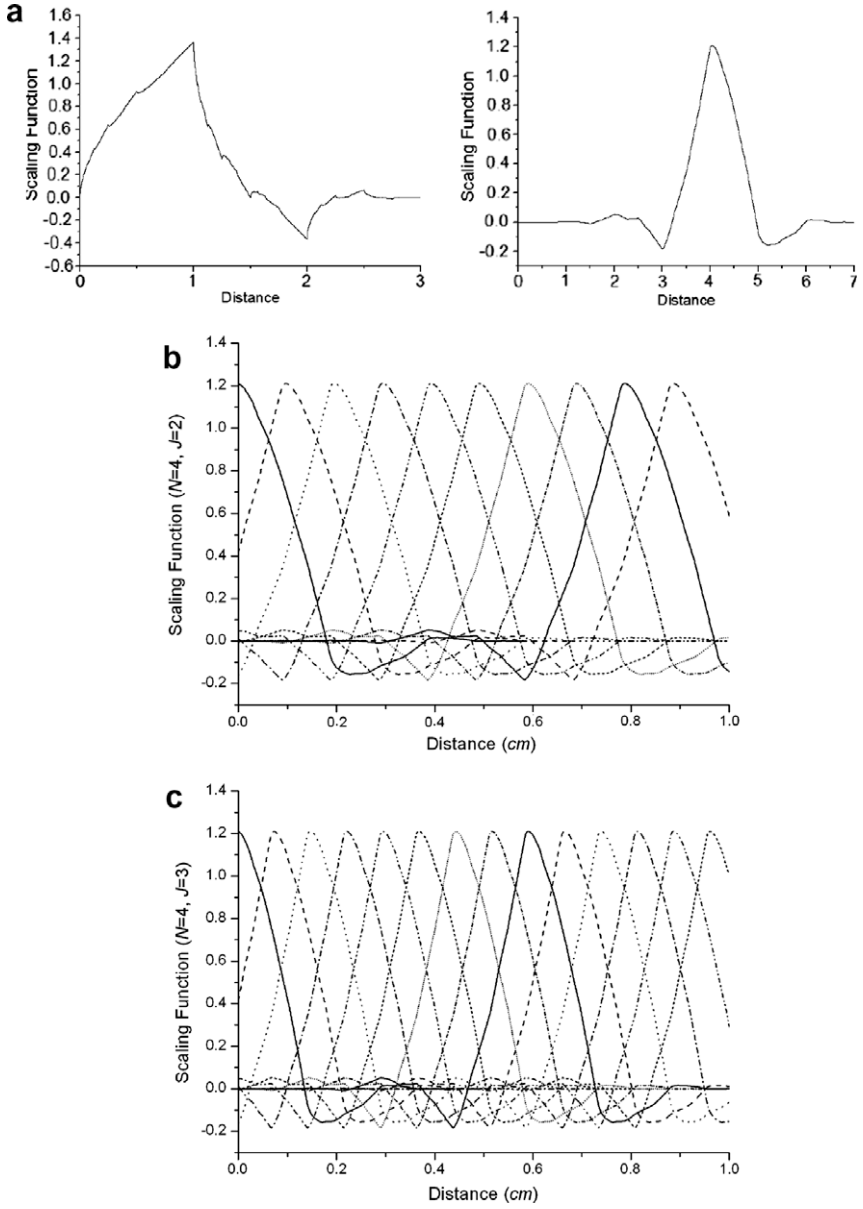

Fig. 1. (a) Distribution of scaling function for $N = 2$ and $N = 4$. (b) Distribution of scaling function for $N = 4$ and $J = 2$ on a unit interval. (c) Distribution of scaling function for $N = 4$ and $J = 3$ on a unit interval.

where P_n is the projection operator. Then, an approximation of the complete wavelet expansion can be written as

$$f_n(t) = \sum_k a_k \varphi_{n,k}(t) \quad 0 \leqslant t < 1 \tag{22}$$

since the scaling functions $\varphi_{n,k}(t)$ are the orthogonal bases of subspace V_n.

Compared with the initial expression consists of the wavelet functions, the scaling function expansion complements a simulation process rather than the decomposition and reconstruction process. Namely, without a specific definition of each component, the set of scaling functions affects as a whole. Moreover, the approximation diminishes the complexity of expansion, where the key is the selection of appropriate dilation order. Fig. 1 illustrated the distributions of Daubechies' scaling functions with different Daubechies order N and dilation order n. The higher Daubechies order possesses better smoothness, continuity and longer compact support. The higher dilation order brings more exact simulation for its more components on a given interval.

3. The model of decoupled S_N and wavelet expansion method

3.1. The first-order Boltzmann transport equation

This paper involves the first-order form of Boltzmann transport equation which does not suffer the singularity in void medium. Define Φ_g is the angular flux in group g, the stable multi-group Boltzmann transport equation can be written as

$$\Omega \frac{\partial \phi_g(r,\Omega)}{\partial r} + \sum_{t,g} \phi_g(r,\Omega) = Q_{f,g}(r,\Omega) + Q_{s,g}(r,\Omega) + S_g(r,\Omega) \tag{23}$$

where r is the spatial variable and Ω is the direction vector as illustrated in Fig. 2. $\sum_t$ is the macro total cross-section in group g.

$Q_{f,g}$ stands for the fission source in group g, which is usually considered as an isotropic item as follows:

$$Q_{f,g} = \frac{\chi_g}{4\pi k} \sum_{g'=1}^{G} \int_{\Omega'} \nu \Sigma_{f,g'} \phi_{g'}(r,\Omega') d\Omega' \tag{24}$$

where k is the eigenvalue, χ_g, $\Sigma_{f,g}$ are the fission spectrum and macro fission cross-section in group g, respectively.

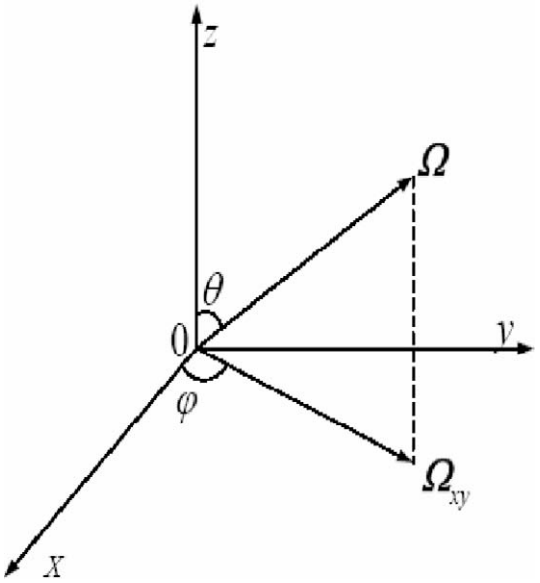

Fig. 2. Cartesian geometry.

Q_{sg} stands for the scattering source in group g, which is considered as an anisotropic item. Usually, the anisotropic scattering source is represented in a Legendre polynomial form with the following formulation:

$$\begin{aligned} Q_{s,g} = {} & \frac{1}{2\pi} \sum_{l=0}^{L} \frac{2l+1}{2} \sum_{g'=1}^{G} \Sigma_{g'-g',l} P_l(\mu) \int_{2\pi} d\varphi' \int_{-1}^{1} P_l(\mu') \phi_{g'}(r,\mu',\varphi') d\mu' \\ & + \frac{1}{\pi} \sum_{l=0}^{L} \frac{2l+1}{2} \sum_{g'=1}^{G} \Sigma_{g'-g,l} \sum_{k=1}^{l} \frac{(l-k)!}{(l+k)!} P_l^k(\mu) \int_{-1}^{1} P_l^k(\mu') d\mu' \\ & \times \int_{2\pi} \cos k(\varphi' - \varphi) \phi_{g'}(r,\mu',\varphi') d\varphi' \end{aligned} \tag{25}$$

where $\Sigma_{g'\text{-}g,l}$ is the macro scattering cross-section from group g' to g. μ and φ are the polar cosine and azimuthal variable, respectively. $P_l(\mu)$ is the Legendre function and $P_l^k(\mu)$ is the associated Legendre function. S_g is the extra source item, which is usually considered to be isotropic.

In general, the wavelet expansion method is similar to the P_N (Sphere Harmonic) method. Therefore, the same puzzle arises in the boundary condition definition, especially for the first-order Boltzmann transport equation. In this paper, an angular subdomain scheme (Cao et al., 2008) is applied to define the boundary condition. This scheme transforms the continuous angular region into several individual subdomains. The wavelets are applied to expand the continuous angular flux in each subdomain. The neighbors are coupled by the boundary condition. The division of angular subdomain is illustrated in Fig. 3.

In this scheme, the angular subdomains are defined in an anticlockwise order. Eight subdomains are divided for the three-dimensional geometry. In this scheme, the boundary conditions are defined as follows

1. The reflective boundary condition

$$\phi_g(r,\Omega) = \phi_g(r,\Omega') \quad r \in \Gamma \wedge n(r) \cdot \Omega < 0 \tag{26}$$

where Ω' is the reflective direction vector of Ω and Γ stands for the boundary. $n(r)$ is the normal direction of point r. In the angular subdomain scheme, the reflective relationship arises between the neighbors, while the angular flux in each subdomain is kept continuous. Then, the boundary condition is transformed to be the definition of relationships between the wavelet expansion coefficients.

2. The vacuum boundary condition

$$\phi_g(r,\Omega) = 0.0 \quad r \in \Gamma \wedge n(r) \cdot \Omega < 0 \tag{27}$$

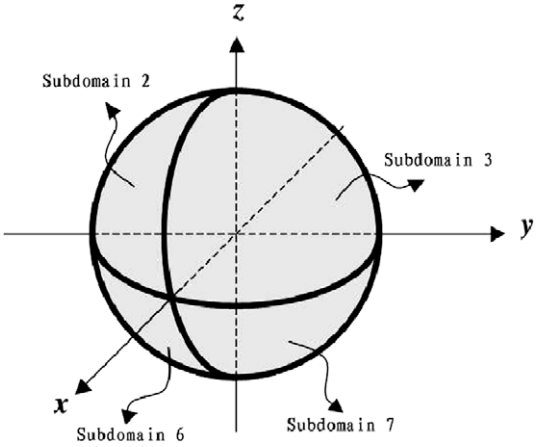

Fig. 3. Division of angular subdomain scheme.

In the angular subdomain scheme, this boundary condition is solved exactly and spontaneously by defining the wavelet expansion coefficients in the incidence subdomain to be zero.

3.2. The angular discretization of Boltzmann transport equation

Based on the angular subdomain scheme, advance transformations are necessary to apply the wavelet expansion in solving the Boltzmann transport equation. Firstly, the angular flux in each subdomain is defined on the interval [0, 1]. Secondly, the azimuthal variable is defined on the interval $[-\pi,\ \pi]$ rather than $[0, 2\pi]$. Here, the angular flux is defined as follows (only angular flux in the uphemisphere is introduced in this section)

$$\phi_g(r,\mu,\varphi)=\begin{cases}\phi_g^1(r,\mu,-\pi+\frac{\pi}{2}\xi)\\ \phi_g^2(r,\mu,-\frac{\pi}{2}\xi)\\ \phi_g^3(r,\mu,\frac{\pi}{2}\xi)\\ \phi_g^4(r,\mu,\pi-\frac{\pi}{2}\xi)\end{cases} \tag{28}$$

where $\mu>0$ and $\xi\in[0,1]$. $\phi_g^1,\phi_g^2,\phi_g^3$ and ϕ_g^4 stand for the angular flux in the first four angular subdomains, respectively.

Previous studies have indicated that the two-dimensional wavelet expansion using a tensor product form is not an ideal approach for the Daubechies' wavelet angular discretization of Boltzmann transport equation (Cao et al., 2008). A new approach to discretize the angular variables is proposed, i.e., the S_N method is applied to discretize the polar variable and the scaling functions are only used to expand the azimuthal variable.

The decoupled scheme is deduced by defining

$$\int_{\Delta\mu_m}\phi_g(r,\mu,\xi)d\mu=\omega_m\phi_{g,m}(r,\xi) \tag{29}$$

and

$$\int_{\Delta\mu_m}\Omega\nabla\phi_g(r,\mu,\xi)d\mu=\omega_m[\Omega\nabla\phi_g(r,\mu,\xi)]_m \tag{30}$$

where ω_m is the S_N weight corresponding to the direction μ_m.

Define the wavelet expansion as

$$\phi_{g,m}(r,\zeta)=\sum_n\psi_{g,mn}(r)\varphi_n(\xi) \tag{31}$$

where $\xi\in[0,1]$. Finally, the expression of discretized equation in each angular subdomain can be deduced by using the Galerkin method, i.e., multiplying each side of Eq. (23) by the same individual scaling function and integrating over the unit interval [0, 1]. Then the final angular discretized form of Eq. (23) is obtained in the angular subdomains as

$$\sqrt{1-\mu_m^2}\sum_n\left[-A_{nn'}\frac{\partial\psi^1_{g,mn}}{\partial x}-B_{nn'}\frac{\partial\psi^1_{g,mn}}{\partial y}\right]+\mu_m\frac{\partial\psi^1_{g,mn'}}{\partial z}+\Sigma_{t,g}\psi^1_{g,mn'}=Q^1_{f,g,mn'}+Q^1_{s,g,mn'}+S^1_{g,mn'} \tag{32}$$

$$\sqrt{1-\mu_m^2}\sum_n\left[A_{nn'}\frac{\partial\psi^2_{g,mn}}{\partial x}-B_{nn'}\frac{\partial\psi^2_{g,mn}}{\partial y}\right]+\mu_m\frac{\partial\psi^2_{g,mn'}}{\partial z}+\Sigma_{t,g}\psi^2_{g,mn'}=Q^2_{f,g,mn'}+Q^2_{s,g,mn'}+S^2_{g,mn'} \tag{33}$$

$$\sqrt{1-\mu_m^2}\sum_n\left[A_{nn'}\frac{\partial\psi^3_{g,mn}}{\partial x}+B_{nn'}\frac{\partial\psi^3_{g,mn}}{\partial y}\right]+\mu_m\frac{\partial\psi^3_{g,mn'}}{\partial z}+\Sigma_{t,g}\psi^3_{g,mn'}=Q^3_{f,g,mn'}+Q^3_{s,g,mn'}+S^3_{g,mn'} \tag{34}$$

$$\sqrt{1-\mu_m^2}\sum_n\left[-A_{nn'}\frac{\partial\psi^4_{g,mn}}{\partial x}+B_{nn'}\frac{\partial\psi^4_{g,mn}}{\partial y}\right]+\mu_m\frac{\partial\psi^4_{g,mn'}}{\partial z}+\Sigma_{t,g}\psi^4_{g,mn'}=Q^4_{f,g,mn'}+Q^4_{s,g,mn'}+S^4_{g,mn'} \tag{35}$$

where $A_{nn'}$ and $B_{nn'}$ are the integrations of directional operator and scaling function, which arises in the Galerkin formulation as

$$A_{nn'}=\int_0^1\cos\left(\frac{\pi}{2}\xi\right)\varphi_n(\xi)\varphi_{n'}(\xi)d\xi \tag{36}$$

$$B_{nn'}=\int_0^1\sin\left(\frac{\pi}{2}\xi\right)\varphi_n(\xi)\varphi_{n'}(\xi)d\xi \tag{37}$$

3.3. The differences between the wavelet function bases and scaling function bases

Ostensibly, the final forms of discretized equations are very similar to the previous one obtained from the wavelet function bases (Cao et al., 2008). The most significant difference is the construction of source items.

As in Eq. (20), the wavelet function expansions consist of average value and contributions from different scales. Source items, including the fission source and scattering source, are generated from the first item of wavelet expansion, which is denoted as the scalar flux. However, the scaling function bases denote an approximate expression of angular flux in a subspace as in Eq. (21). All items contribute to the scalar flux, which are inevitably obtained by using numerical integrations. Then, the scalar flux is represented as

$$\overline{\phi(r)}=\sum_m w_m\sum_n w_n\sum_{i=1}^{8}\psi^i_{m,n}(r) \tag{38}$$

where w_m is the weight of Gauss integration in [0, 1] and w_n is the integration of individual scaling function defined as

$$w_n=\int_0^1\varphi_n(\xi)d\xi \tag{39}$$

Therefore, the fission source is represented simply in the wavelet expansion form

$$Q_{f,g,mn}=w_n\frac{\chi_g}{4\pi k}\sum_{g'=1}^{G}\nu\Sigma_{f,g'}\sum_{m'}w_{m'}\sum_{n'}w_{n'}\sum_{i=1}^{8}\psi^i_{g',m'n'}(r) \tag{40}$$

Since the anisotropic scattering is considered in this paper, special treatments are necessary to transform the common expression of scattering source into the one available in the decoupled angular discretization scheme. This work also starts with the S_N discretization of polar variable. According to Eq. (25), the scattering source can be rewritten as

$$\begin{aligned}Q_{s,g,m}=&\frac{1}{2\pi}\sum_{l=0}^{L}\frac{2l+1}{2}\sum_{g'=1}^{G}\Sigma_{g'-g',l}P_l(\mu_m)\int_{2\pi}\left[\sum_{m'}w_{m'}P_l(\mu'_m)\phi_{g',m'}(r,\varphi')+\sum_{m'}w_{m'}P_l(-\mu'_m)\phi_{g',m'}(r,\varphi')\right]d\varphi'\\&+\frac{1}{\pi}\sum_{l=0}^{L}\frac{2l+1}{2}\sum_{g'=1}^{G}\Sigma_{g'-g,l}\sum_{k=1}^{l}\frac{(l-k)!}{(l+k)!}P_l^k(\mu_m)\\&\times\int_{2\pi}\cos k(\varphi'-\varphi)\left[\sum_{m'}w_{m'}P_l^k(\mu'_m)\phi_{g',m'}(r,\varphi')+\sum_{m'}w_{m'}P_l^k(-\mu'_m)\phi_{g',m'}(r,\varphi')\right]d\varphi'\end{aligned} \tag{41}$$

Take the first angular subdomain for example, the scattering source can be represented as:

$$
\begin{aligned}
Q^1_{s,g,mn} = w_n \times \sum_{l=0}^{L} \frac{2l+1}{8} \sum_{g'=1}^{G} \Sigma_{g'-g',l} P_l(\mu_m) \\
\times \left[\sum_{m'} w_{m'} P_l(\mu'_m) \sum_{n'} w_{n'} \sum_{i=1}^{4} \psi^i_{m',n'}(r) + \sum_{m'} w_{m'} P_l(-\mu'_m) \right. \\
\left. \times \sum_{n'} w_{n'} \sum_{i=5}^{8} \psi^i_{g',m'n'}(r) \right] + \int_0^1 \cos\left(-k\pi + \frac{\pi}{2}\xi\right) \varphi_n(\xi) d\xi \\
\times \sum_{l=0}^{L} \frac{2l+1}{4} \sum_{g'=1}^{G} \Sigma_{g'-g,l} \sum_{k=1}^{l} \frac{(l-k)!}{(l+k)!} P^k_l(\mu_m) \times \sum_{m'} w_{m'} P^k_l(\mu'_m) \\
\times \sum_{n'} \int_0^1 \cos\left(-k\pi + \frac{\pi}{2}\xi'\right) \varphi_{n'}(\xi') d\xi' \psi^1_{g',m'n'}(r) + \ldots \\
+ \int_0^1 \cos\left(-k\pi + \frac{\pi}{2}\xi\right) \varphi_n(\xi) d\xi \times \sum_{l=0}^{L} \frac{2l+1}{4} \sum_{g'=1}^{G} \Sigma_{g'-g,l} \\
\times \sum_{k=1}^{l} \frac{(l-k)!}{(l+k)!} P^k_l(\mu_m) \times \sum_{m'} w_{m'} P^k_l(-\mu'_m) \\
\times \sum_{n'} \int_0^1 \cos\left(k\pi - \frac{\pi}{2}\xi'\right) \varphi_{n'}(\xi') d\xi' \psi^8_{g',m'n'}(r) \qquad (42)
\end{aligned}
$$

Since k is a variational integer, it is necessary to represent Eq. (41) distinguishingly, judging whether k is an even or odd.

Besides the differences in the source definition, another difference is the relationship of wavelet expansion coefficients. The new bases are obtained from the scaling function in a given scale. Due to the compact support and orthonormal properties, the scaling functions possess non-zero integrations only in their neighboring region. This is a very important difference from the wavelet basis function, which consists of not only the scaling functions but also the wavelet functions in different scales, which bring more non-zero integrations from different scales. As a result, the amount of coupled expansion coefficients decreases sharply for the scaling function and less coupling arise in Eqs. (32)–(35). It results much higher efficiency and better computational stability in solving the set of coupled equations.

The third difference is the calculation of wavelet expansion coefficients defined in Eqs. (36) and (37). Since there are no contributions from different scales, the numerical integrations become easier and more efficient while only the scaling functions are considered. Meanwhile, the calculation of wavelet integrations considers only the judgement of translation ranges. It makes the integration range much shorter.

3.4. The spatial discretization

There are many methods to solve the angular discretized equations as in Eqs. (32)–(35). In this paper, we apply the finite difference method (FDM) to solve them. There are two approaches to decouple the wavelet expansion coefficients, one is an iterative scheme (Cao et al., 2008) and the other is a step scheme. Here we choose the latter one, i.e., calculate the coupled wavelet expansion coefficients directly and simultaneously in every source iteration step.

The spatial discretization starts with the integrations on meshes. Define Δx_i, Δy_j and Δz_k are the length, width and height of mesh (i, j, k), respectively. The spatial discretized form of Eq. (32) is written as

$$
\begin{aligned}
\sum_n \left[-A_{nn'} (\psi^1_{g,mn,i+1/2,j,k} - \psi^1_{g,mn,i-1/2,j,k}) \Delta y_j \Delta z_k \right. \\
\left. - B_{nn'} (\psi^1_{g,mn,ij+1/2,k} - \psi^1_{g,mn,ij-1/2,k}) \Delta x_i \Delta z_k \right] \\
+ \left[\mu_m (\psi^1_{g,mn',i,j,k+1/2} - \psi^1_{g,mn',i,j,k-1/2}) + \Sigma_{t,g} \psi^1_{g,mn',i,j,k} \right] \Delta x_i \Delta y_j \Delta z_k \\
= \left[Q^1_{f,g,mn',i,j,k} + Q^1_{s,g,mn',i,j,k} + S^1_{g,mn',i,j,k} \right] \Delta x_i \Delta y_j \Delta z_k \qquad (43)
\end{aligned}
$$

And the diamond approximations are applied in the following form:

$$
\begin{aligned}
\psi^1_{g,mn',i,j} &= \frac{\psi^1_{g,mn',i+1/2,j,k} + \psi^1_{g,mn',i-1/2,j,k}}{2} \\
&= \frac{\psi^1_{g,mn',ij+1/2,k} + \psi^1_{g,mn',ij-1/2,k}}{2} \\
&= \frac{\psi^1_{g,mn',i,j,k+1/2} + \psi^1_{g,mn',i,j,k-1/2}}{2} \qquad (44)
\end{aligned}
$$

A sweep scheme is used instead of constructing a matrix to obtain the wavelet expansion coefficients $\psi^1_{g,mn',ij}$ in every mesh.

4. The numerical results

A multi-group neutron transport FORTRAN code package, WAVTRAN, based on the model described in Section 3 is developed, considering the anisotropic scattering and three-dimensional geometry. Up to P_5 anisotropic scattering is considered in this code package. Several test problems are calculated using this code package. Typical neutron transport benchmarks are calculated in Sections 4.1–4.4, which demonstrate the feasibility and accuracy of WAVTRAN in two-dimensional, anisotropic scattering and three-dimensional problems. Also in Section 4.2, the angular reconstruction is given to compare the result with previous study (Cao et al., 2008) and demonstrate the effectiveness of eliminating edge effect of wavelets in this work. Additionally, two problems considering the ray effect and high-order angular approximation are given in Sections 4.5 and 4.6, respectively. They are expected to demonstrate that the WAVTRAN can not only handle the typical problems but also effective in the challenging problems. All the calculations in this paper are performed on the PC (Pentium 4, 2.66 GHz). The number of angular unknowns is determined by $T = M \times 2^{J+2}$, where M is the number of polar direction and J is the dilation order used in the azimuthal expansion.

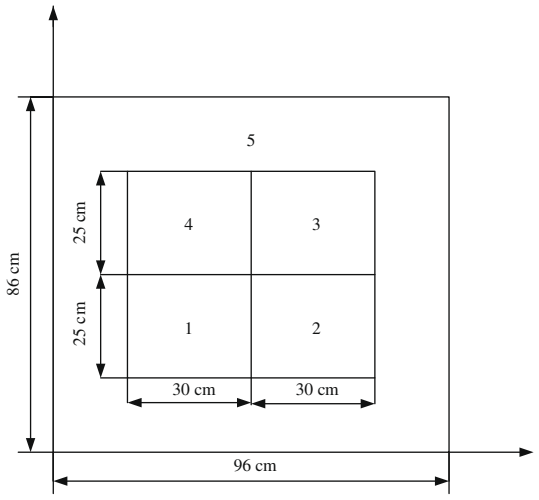

Fig. 4. Geometry of IAEA benchmark.

Table 1
Cross-sections of IAEA benchmark.

Region	Σ_t	Σ_s	$\nu\Sigma_f$
1	0.6	0.53	0.079
2	0.48	0.2	0.0
3	0.7	0.66	0.043
4	0.65	0.5	0.0
5	0.9	0.89	0.0

Table 2
Results of IAEA benchmark.

	No. of angular unknowns	Average flux					K_{eff}	CPU time (s)
		Region 1	Region 2	Region 3	Region 4	Region 5		
SURCU	–	0.0169	0.00013	0.00004	0.00030	0.00079	1.0083	–
DOT4	12 (S_4)	0.0169	0.00013	0.00004	0.00029	0.00079	1.0088	126.92
Wavelet	32 ($2 \times 2^{2+2}$)	0.0170	0.00013	0.00004	0.00030	0.00080	1.0089	106.36
	48 ($3 \times 2^{2+2}$)	0.0170	0.00013	0.00004	0.00030	0.00080	1.0089	163.49
	64 ($2 \times 2^{3+2}$)	0.0170	0.00013	0.00004	0.00030	0.00080	1.0088	463.53

4.1. IAEA benchmark

This benchmark (Stepanek et al., 1983), designed for IAEA advanced reactor neutron transport calculation, is a two-dimensional problem with five regions. The geometry and cross-section data are given in Fig. 4 and Table 1, respectively. All sides are the vacuum boundary conditions. The references are given by SURCU (Stepanek et al., 1983) and DOT4 (Rhoades and Mynatt, 1979), which are based on the integral transport method and S_N method, respectively. The same meshes (96×86) are used in both WAVTRAN and DOT4 with S_4 angular approximation.

The results of WAVTRAN are shown in Table 2. Compared with the references, the results of WAVTRAN are sufficiently accurate, even though low angular order is applied. Obviously, the higher order in the azimuthal direction will significantly increase the cost of CPU time.

4.2. Issa benchmark

This benchmark (Issa et al., 1986) is an extended two-dimensional eigenvalue problem, which is applied to test the high-order anisotropic option in WAVTRAN. The calculations adopted in this problem consist of two parts, one with the isotropic scattering and the other with the anisotropic scattering. Up to P_5 scattering is used as shown in Table 3. The reflective and vacuum boundary conditions are applied as in Fig. 5. Fifty rectangle meshes are used in the two-dimensional calculation, compared with the references given by ANISIN (Engle, 1973) S_{16} approximation (equivalent 25 meshes in the one-dimensional calculation) as in Table 4.

Table 3
Cross-sections of Issa benchmark.

	Σ_t	$\Sigma_{s,0}$	$\Sigma_{s,1\text{-}5}$	$\nu\Sigma_f$
Fuel	1.1	0.6	0.1	1.0
Coolant	0.95	0.55	0.15	0.0

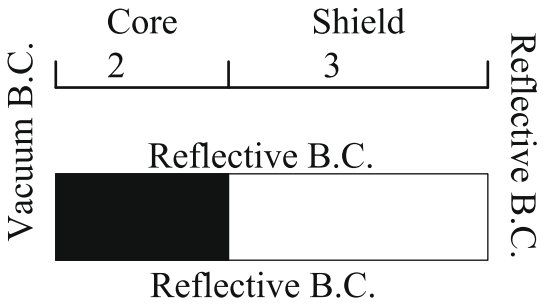

Fig. 5. Geometry of Issa benchmark and its extended two-dimensional form.

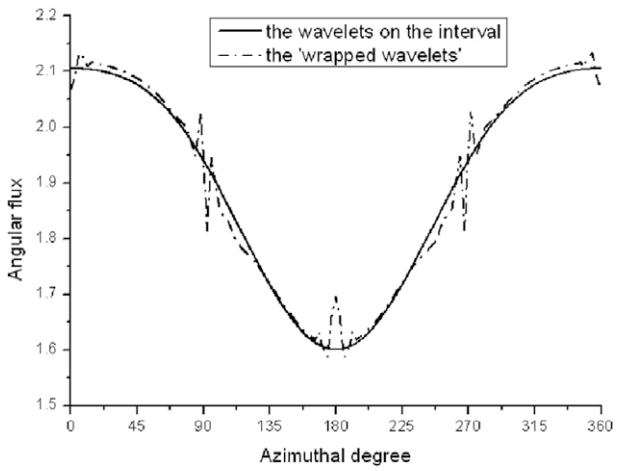

Fig. 6. Comparison of angular flux distribution obtained by different wavelet bases.

Two improvements of WAVTRAN are demonstrated. Firstly, due to the sparse coupling of wavelet expansion coefficients, the computational cost is improved reflected on the decrease of CPU time. Secondly, due to adopting the improved wavelets on the interval, the accuracy is significantly improved as in Table 4 and Fig. 6, where the edge effect induced by the 'wrapped wavelets' is absolutely eliminated.

4.3. Simplified LWR benchmark

This benchmark (Xie and Dorning, 1986) represents a three-dimensional simplified reactor. The reactor consists of a fuel region having dimensions of $10 \times 10 \times 10$ cm and a reflector region of

Table 5
Cross-sections of simplified LWR benchmark.

	Σ_t	Σ_s	$\nu\Sigma_f$
Fuel	1.0	0.93	0.117
Coolant	0.8	0.792	0.0

Table 4
Results of Issa benchmark.

	ANISIN S_{16}	"Wrapped" wavelet basis function[a]	WAVTRAN		
No. of angular unknowns	16	64 ($2 \times 2^{3+2}$)	64 ($2 \times 2^{3+2}$)	128 ($2 \times 2^{4+2}$)	192 ($3 \times 2^{4+2}$)
K_{eff}	1.6781	1.6834	1.6779	1.6780	1.6784
CPU time (s)	–	15.812	0.203	0.532	0.906

[a] Another approach to adopt wavelets in the angular discretization (Cao et al., 2008).

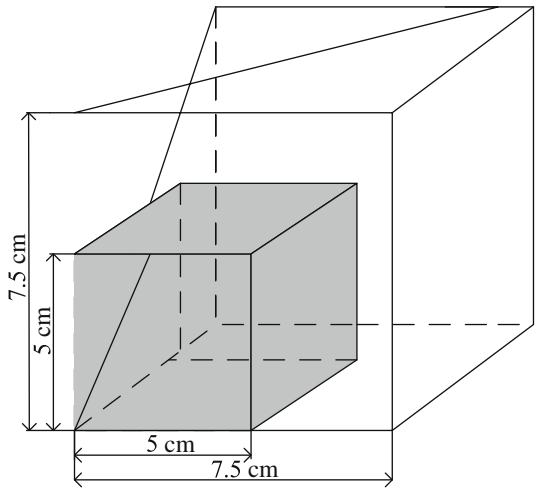

Fig. 7. Geometry of simplified LWR benchmark.

2.5 cm thickness outside each side of the fuel region. The overall dimensions are $15 \times 15 \times 15$ cm. The cross-section data is given in Table 5. The vacuum boundary conditions are applied on each side. In this calculation, a 1/8 symmetry structure are applied as illustrated in Fig. 7.

The results of WAVTRAN at different angular order are given in Table 6, and compared with the results obtained by use of DNTM, a S_N code based on the nodal method (Xie and Dorning, 1986). Different angular approximations are applied with the same $9 \times 9 \times 9$ nodes. Due to the diamond difference method, here we use $15 \times 15 \times 15$ fine meshes in this paper. Reference solution is obtained by using a multi-group Monte Carlo method with 10,000 particles in 250 histories. The comparison shows that WAVTRAN obtains more accurate results with the increase of angular refinement. However, the refinement will significantly increase the computational time cost.

4.4. KUCA benchmark

This is a three-dimensional KUCA (Kyoto University Critical Assembly) LWR benchmark done by Takeda and Ikeda (1991).

Table 7
Results of KUCA benchmark.

	No. of angular unknowns	K_{eff}		Control rod value
		Control rod out	Control rod in	
		0.9778	0.9624	1.64E−02
Monte Carlo	–	±0.0005[a]	±0.0005	±7.00E−04
S_4	24	0.9766	0.9622	1.54E−02
S_8	80	0.9772	0.9623	1.58E−02
WAVTRAN	32 ($2 \times 2^{2+2}$)	0.9784	0.9612	1.83E−02
	64 ($4 \times 2^{2+2}$)	0.9773	0.9613	1.70E−02

[a] Standard variance.

Three regions considering the core, reflector and control rod are included in a structure having dimensions of $10 \times 10 \times 10$ cm. Fig. 8 illustrates the structure and corresponding boundary condition by describing the X–Y and X–Z cross-section, separately. Two group cross-section data of different materials is cited from the literature (Takeda and Ikeda, 1991). Two conditions including the control rod in and control rod out are calculated to determine the control rod value.

Table 7 gives the results of WAVTRAN with different angular order and the same $25 \times 25 \times 25$ rectangle meshes. Reference solutions are obtained by using also the multi-group Monte Carlo method and S_N method with S_4, S_8 approximation and the same $25 \times 25 \times 25$ rectangle meshes. From the comparisons, the WAVTRAN is demonstrated to be accurate enough to handle the typical three-dimensional calculation. The angular refinement will actually improve the results.

4.5. Ray effect problem

This benchmark (Zekeriya and Spinrad, 1990) is a one-group two-region fixed source problem which was proven to exhibit the ray effect for S_N method. The system is a 3×3 cm square with a unit source region as in Fig. 9. The cross-sections are given in Table 8. Reflective boundary conditions are applied in all the sides.

Fig. 10 illustrates the distribution of scalar flux along the bottom side. The references are given from TWOTRAN with S_8 approximation and SK_N method (Zekeriya and Spinrad, 1990) with SK_5 approximation. Due to the ray effect, the result of TWOTRAN represents strong oscillation. But the wavelet result (Daubechies order

Table 6
Results of simplified LWR benchmark.

	Ref.	DNTM			WAVTRAN		
No. of angular unknowns	–	8	24	80	64 ($2 \times 2^{3+2}$)	128 ($4 \times 2^{3+2}$)	256 ($8 \times 2^{3+2}$)
K_{eff}	0.97350	0.97527	0.97629	0.97673	0.97254	0.97306	0.97327
CPU time (s)	–	–	–	–	9.67	23.67	87.75

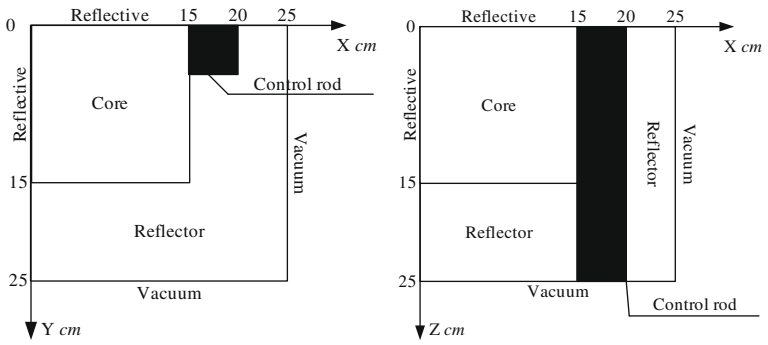

Fig. 8. Geometry of KUCA benchmark.

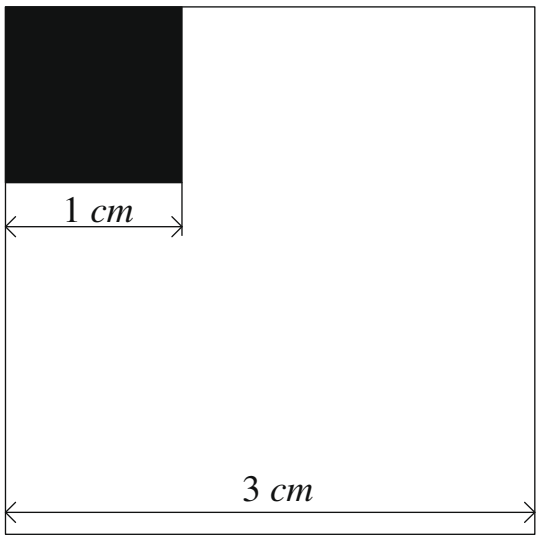

Fig. 9. Geometry of ray effect problem.

Table 8
Cross-sections of ray effect problem.

Region	Σ_t	Σ_s	S
Source	1.0	0.5	1.0
Shield	1.0	0.25	0.0

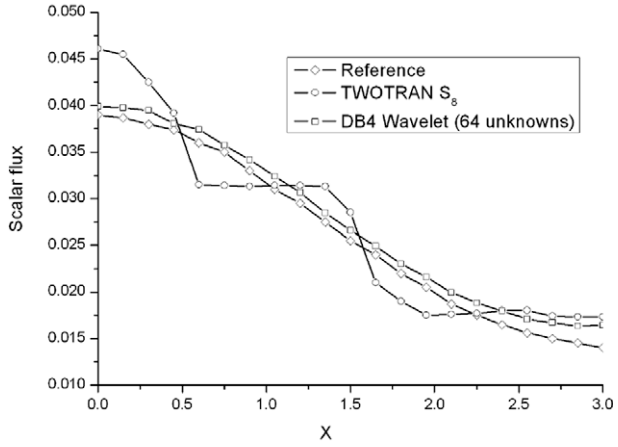

Fig. 10. Comparison of scalar flux distribution of ray effect problem.

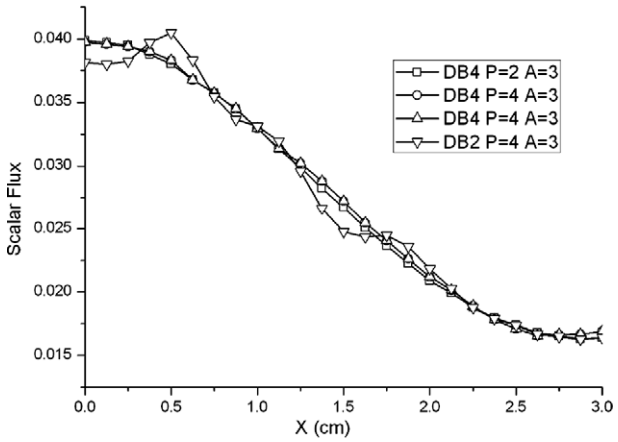

Fig. 11. Comparison of scalar flux distribution with different order (DB, P and A stand for the Daubechies order, polar order and azimuthal order, respectively).

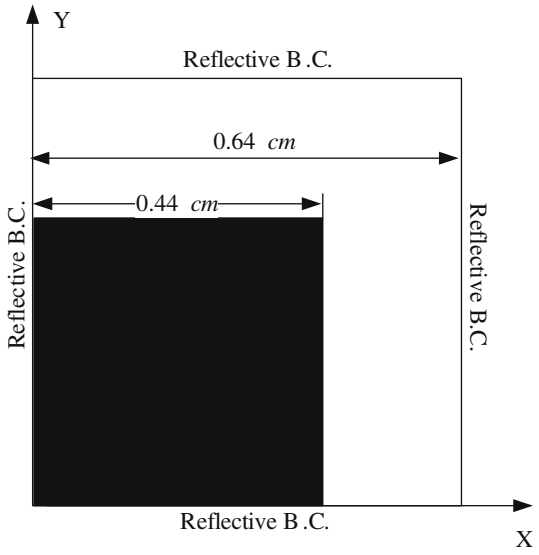

Fig. 12. Geometry of high-order angular approximation problem.

Table 9
Results of high-order angular approximation problem by DOT4.

	Ref.	S_4	S_8	S_{12}	S_{16}
No. of angular unknowns	–	16	48	96	160
K_{eff}	1.12843	1.11605	1.11865	1.12041	1.12158

is equal to four and 64 angular unknowns needed) represents smooth distribution. Fig. 11 gives the differences between different polar, azimuthal and Daubechies order. According to the figures, different polar and azimuthal order does not affect much but low Daubechies order will suffer the ray effect. Fortunately, higher Daubechies order does not affect the computational cost, since the number of angular unknowns depends on the polar and azimuthal order but not on the Daubechies order.

4.6. High-order angular approximation problem

This problem is designed based on the investigations of MOX pin cell heterogenous calculation (Smith, 2001). The neutron flux presents highly anisotropic distribution in such problem, which requires high-order angular approximation. To facilitate the calculation with different spatial approximation methods, we approximate the geometry by using square fuel pins as shown in Fig. 12. Also, the cladding region and void gap are ignored for simplifying the calculations. A set of seven group cross-section is obtained in the MOX benchmark problems issued by Cho (http://nurapt.kaist.ac.kr/lab/kr/Eng/top3.htm).

The reference is given by a multi-group Monte Carlo method with 20,000 particles in 250 histories. The eigenvalues obtained by use of DOT4 with increasing S_N order are given in Table 9. Up to S_{16} angular approximation is given. The results demonstrate that very high-order angular approximation is necessary. Compared with them, the results using WAVTRAN as in Table 10 are much more accurate even though using the low order expansion, which demonstrate that the wavelet-based method is more suitable and

Table 10
Results of high-order angular approximation problem by WAVTRAN.

	Ref.	WAVTRAN					
No. of angular unknowns	–	64 ($2 \times 2^{3+2}$)	96 ($3 \times 2^{3+2}$)	128 ($4 \times 2^{3+2}$)	128 ($2 \times 2^{4+2}$)	192 ($3 \times 2^{4+2}$)	256 ($4 \times 2^{4+2}$)
K_{eff}	1.12843	1.12524	1.12611	1.12655	1.12594	1.12686	1.12729

efficient than traditional angular approximation schemes in solving such problems.

5. Conclusions

This paper focuses on the improvements of decoupled S_N and wavelet expansion angular discretization scheme. The scaling function is applied as basis function instead of the wavelet function. It results sparse coupling between the expansion coefficients and is good for improving the computational efficiency. The Daubechies' wavelets on the interval are applied instead of the 'wrapped wavelets'. It is a special approach for eliminating the edge effect of wavelet expansion and improves the accuracy. With the new basis function, the model considering three-dimensional calculation and anisotropic scattering are deducted to complete the angular discretization scheme.

A FORTRAN code package WAVTRAN is developed based on the improvements. Numerical tests so far have indicated that the wavelet-based angular discretization scheme can handle both two-dimensional and three-dimensional calculations, including the cases considering anisotropic scattering. Moreover, the numerical tests demonstrate that the application of sparsely coupled basis function significantly improves the computational efficiency, and the wavelets on the interval result more accurate calculations for essentially eliminating the edge effect.

Further calculation indicates that the wavelet-based angular discretization scheme also suffers ray effect while low Daubechies order is applied. But the higher Daubechies order mitigates this phenomenon significantly. Also, a high-order angular approximation problem is involved in this paper, which demonstrates that the wavelet-based angular discretization scheme can handle angular complications more effectively than the traditional methods.

However, the source iteration method is still applied in the decoupled angular discretization scheme without any acceleration technique. Available acceleration method based on the wavelet expansion requires further investigations.

Acknowledgement

This research was carried out under the financial support of the National Science Foundation of China (Approved Nos. 10605017 and 10875094).

References

Buchan, A.G., Pain, C.C., et al., 2005. Linear and quadratic octahedral wavelets on the sphere for angular discretisations of the Boltzmann transport equation. Ann. Nucl. Energy 32, 1224–1273.

Cao, L., Wu, H., Zheng, Y., 2008. Solution of neutron transport equation using Daubechies' wavelet expansion in the angular discretization. Nucl. Eng. Des. 238, 2292–2301.

Carron, I., 1999. Solving the transport equation with spline wavelets. Technical Report, Dep. of Nuclear Eng., Texas A&M University, College Station, Texas.

Cho, N.Z., Cao, L., 2006. Wavelet-theoretic method for solution of neutron transport equation. In: Transactions of the Korean Nuclear Society Spring Meeting, Chuncheon, Korea, May 25–26, 2006.

Cohen, A., Daubechies, I., Vial, P., 1993. Wavelets on the interval and fast wavelet transforms. Appl. Comput. Harmon. Anal. 1, 54–81.

Daubechies, I., 1992. Ten Lectures on Wavelets. SIAM, Philadelphia, PA.

Engle, W.W., 1973. A User's Manual for ANISN. USAEC Report KI-1693 (1967); ANISN-ORNL, A One-Dimensional Discrete Ordinates Transport Code. Oak Ridge National Laboratory Report CCC-254.

Guven, O., Bayazitoglu, Y., 2003. The radiative transfer solution of a rectangular enclosure using angular domain discrete wavelets. Int. J. Heat Mass Transfer 46, 687–694.

Issa, J.G., Riyait, N.S., Goddard, A.J.H., et al., 1986. Multigroup application of the anisotropic FEM code FELTRAN to one, two, three-dimensional and R-Z problems. Prog. Nucl. Eng. 18 (1), 251–264.

Newland, D.E., 1993. An Introduction to Random Vibrations, Spectral & Wavelet Analysis. John Wiley and Sons, New York.

Rhoades, W.A., Mynatt, F.R., 1979. The DOT-IV: Two-Dimensional Discrete Ordinates Transport Code. Oak Ridge National Laboratory.

Smith, M.A., 2001. Comparison of angular approximations for PWR cell calculations. Trans. Am. Nucl. Soc. 84, 90–91.

Stepanek, J., Auerbach, T., Haelg, W., 1983. Calculation of four thermal reactor benchmark problems in X–Y geometry, EPRI NP-2855.

Takeda, T., Ikeda, H., 1991. 3-D neutron transport benchmarks. J. Nucl. Sci. Technol. 28 (7), 656–669.

Xie, Z., Dorning, J.J., 1986. A discrete nodal method for three-dimensional neutron transport numerical calculations. Chinese J. Nucl. Sci. Eng. 6 (4), 311–322.

Zekeriya, A., Spinrad, B.I., 1990. The SK_N method I: a high-order transport approximation to neutron transport problems. Nucl. Sci. Eng. 106, 471–479.